

Hall drift in the stratified crusts of neutron stars

Rainer Hollerbach¹*† and Günther Rüdiger²

¹Brandenburgische Technische Universität Cottbus, LAS, Fakultät 3, 03013 Cottbus, Germany

²Astrophysikalisches Institut Potsdam, An der Sternwarte 16, 14482 Potsdam, Germany

Accepted 2003 October 16. Received 2003 September 30; in original form 2003 July 23

ABSTRACT

We extend our previous numerical model of Hall drift in neutron stars (Hollerbach & Rüdiger 2002) to include variations in density across the depth of the crust. For purely toroidal fields, the results are in perfect agreement with the analytic model of Vainshtein, Chitre & Olinto (2000), who showed that the field would develop very fine structures, which would cause it to decay on the Hall time-scale rather than the much longer ohmic time-scale. However, if we include poloidal fields (which were not considered by Vainshtein et al.), the behaviour is rather different. The field still develops fine structures, but not as fine as before, scaling roughly as $R_B^{-1/2}$ rather than the R_B^{-1} scaling obtained for purely toroidal fields (where the Hall parameter R_B measures the ratio of the ohmic time-scale to the Hall time-scale). As a result, the field still decays considerably faster than if ohmic decay alone were acting, but ultimately still on the ohmic time-scale. This is true even if the initial poloidal field is much weaker than the initial toroidal field (with the sign of the toroidal field also playing an important role). Finally, we consider the possible implications for the magnetic fields of real neutron stars.

Key words: stars: magnetic fields – stars: neutron.

1 INTRODUCTION

The Hall effect is becoming increasingly recognized as a potentially important ingredient in the evolution of astrophysical magnetic fields. This is particularly true in isolated neutron stars, where it is likely to be the dominant mechanism. The key papers in this case are Jones (1988), who was the first to consider Hall drift in neutron stars at all, and Goldreich & Reisenegger (1992), who explored in more detail how it might affect the evolution of the field. In particular, they suggested that Hall drift could lead to a rapid decay of the field, on a $\sim 10^8$ year time-scale for a typical 10^{12} G radio or X-ray pulsar, by cascading magnetic energy to sufficiently short length-scales to where ohmic decay (which otherwise only acts on $\sim 10^{10}$ year time-scales) can efficiently eliminate it.

Following this suggestion, a number of authors (Shalybkov & Urpin 1997; Urpin & Shalybkov 1999; Hollerbach & Rüdiger 2002) performed detailed numerical calculations to see if this decay enhancement mechanism really works. However, all three found that although Hall drift does indeed have a significant influence on the evolution of the field, in no case did that influence amount to decay on a time-scale significantly faster than ordinary ohmic decay.

Before concluding though that this decay enhancement does not work after all, one should bear in mind that in real neutron stars, there

are a number of additional features not included in these idealized numerical models, and that some of these may combine with the basic Hall effect in interesting and unexpected ways. For example, one feature not included in these previous models is the very strong density variation found in the crusts of neutron stars; Vainshtein et al. (2000) have shown that this not only alters the Hall term in the governing equation, but that it does so in a way that may indeed lead to very rapid decay.

This Vainshtein et al. model was idealized in other ways though, most significantly in only including toroidal fields (attempting to include poloidal fields as well would have made the equations analytically intractable). The purpose of this work therefore is to include density variations in our numerical model (Hollerbach & Rüdiger 2002, subsequently referred to as Paper I). Being purely numerical, this model can more easily cope with poloidal as well as toroidal fields. As in Paper I, we start with low-order free-decay modes or simple linear combinations thereof as initial conditions, and then study the subsequent evolution and decay. For purely toroidal initial conditions (for which the field remains purely toroidal), we obtain results in perfect agreement with Vainshtein et al., and, in particular, find that the field decays on the Hall time-scale rather than the ohmic time-scale. For a purely poloidal initial condition, however, the situation is very different. Even though a toroidal field is immediately induced as well, and does indeed attempt to establish the current sheet necessary for this very rapid decay, the presence of the poloidal field prevents this from happening. As the next step, we therefore investigate how much initial poloidal field is necessary before this Vainshtein et al. mechanism is no longer operating even

*Permanent address: Department of Mathematics, University of Glasgow, Glasgow G12 8QW.

†E-mail: rh@maths.gla.ac.uk

qualitatively, and find that surprisingly little – as little as a few per cent – can already be sufficient to disrupt it. Finally, we discuss some of the implications for real neutron stars.

2 EQUATIONS

As in Paper I, the equation to be solved is

$$\frac{\partial \mathbf{B}}{\partial t} = -\nabla \times \left[\frac{c}{4\pi n e} (\nabla \times \mathbf{B}) \times \mathbf{B} \right] - \nabla \times \left[\frac{c^2}{4\pi \sigma} \nabla \times \mathbf{B} \right], \quad (1)$$

where n is the electron number density, σ the conductivity, e the electron charge and c the speed of light. Non-dimensionalizing according to

$$r = r_o r^*, \quad t = \frac{4\pi n_o e r_o^2}{c B_o} t^*, \quad \mathbf{B} = B_o \mathbf{B}^*, \quad (2)$$

where r_o is the radius of the star, B_o a typical field strength, and $n_o = n(r_o)$, we obtain (after dropping the asterisks again)

$$\frac{\partial \mathbf{B}}{\partial t} = -\nabla \times [f(r)(\nabla \times \mathbf{B}) \times \mathbf{B}] + R_B^{-1} \nabla^2 \mathbf{B}, \quad (3)$$

where

$$f(r) = \frac{n(r_o)}{n(r)}, \quad R_B = \frac{\sigma B_o}{n_o e c}, \quad (4)$$

and, as in Paper I, we are still taking σ to be constant.

That is, the only difference between Paper I and here is the inclusion of this function $f(r)$ measuring the radial density stratification; whereas we took $f = 1$ in Paper I, here we wish to consider the effect of non-constant f . Now, in a real neutron star, the density increases by perhaps as much as five orders of magnitude over the depth of the crust (Shapiro & Teukolsky 1983). This density ratio f should therefore vary as $\exp[k(r - r_o)]$, with k sufficiently large that f drops from 1 at the outer boundary to essentially 0 at the inner. Unfortunately, for k greater than 16 or so (corresponding to a drop-off of merely 1 to 0.02 between $r_o = 1$ and $r_i = 0.75$) the ever shorter e-folding depth led to problems with the numerical resolution. Instead of this exponential profile, we therefore took

$$f = \left(\frac{r - r_i}{r_o - r_i} \right)^2, \quad (5)$$

thereby matching the correct limiting values $f(r_o) = 1$ and $f(r_i) = 0$, but with the variation in between distributed somewhat more smoothly, rather than strongly concentrated at the outer boundary. A few runs were also done with various other profiles, and indicate that the results are insensitive to the precise details of how f drops from 1 to 0, or whether it drops all the way to 0, rather than some very small but non-zero value. [Note in particular how $f(r_i) = 0$ implies that $n(r_i)$ is infinite, rather than merely $\sim 10^5$ times greater than $n(r_o)$. Because the relevant quantity in equation (1) is n^{-1} though, this causes no problems.]

Incidentally, we note also that in real neutron stars, the conductivity σ varies with depth just as surely as the density does (although by only two or three orders of magnitude). Nevertheless, we take it to be constant here, for two reasons. First, to facilitate comparison with the results of Vainshtein et al., who also considered variations in density only. Second, since the ohmic decay term is small compared to the Hall term, it is plausible anyway that spatial variations in the precise decay coefficient would also have a relatively small effect. Ultimately though, as we move towards increasingly realistic models, variations in σ will also have to be included.

Returning to equation (3), decomposing \mathbf{B} into toroidal and poloidal components

$$\mathbf{B} = \mathbf{B}_t + \mathbf{B}_p = B \hat{\mathbf{e}}_\phi + \nabla \times (A \hat{\mathbf{e}}_\phi), \quad (6)$$

we obtain

$$\frac{\partial A}{\partial t} = -\hat{\mathbf{e}}_\phi \cdot f[(\nabla \times \mathbf{B}_t) \times \mathbf{B}_p] + R_B^{-1} D^2 A, \quad (7)$$

$$\frac{\partial B}{\partial t} = -\hat{\mathbf{e}}_\phi \cdot \nabla \times f[(\nabla \times \mathbf{B}_p) \times \mathbf{B}_p + (\nabla \times \mathbf{B}_t) \times \mathbf{B}_t] + R_B^{-1} D^2 B, \quad (8)$$

where $D^2 = \nabla^2 - 1/(r \sin \theta)^2$.

Expanding A and B in terms of associated Legendre functions

$$A = \sum A_l P_l^{(1)}(\cos \theta), \quad B = \sum B_l P_l^{(1)}(\cos \theta), \quad (9)$$

the insulating boundary conditions at r_o yield

$$\left(\frac{d}{dr} + \frac{l+1}{r} \right) A_l = 0, \quad (10)$$

$$B = 0. \quad (11)$$

Note in particular how condition (10) matching to an external potential field depends on l .

Matching to a superconducting interior yields the boundary conditions

$$A = 0 \quad (12)$$

$$\frac{f}{r \sin \theta} \frac{\partial}{\partial \theta} (B \sin \theta) B + R_B^{-1} \frac{1}{r} \frac{\partial}{\partial r} (B r) = 0 \quad (13)$$

at r_i . In fact, because $f(r_i) = 0$, (13) simplifies to just $\partial(Br)/\partial r = 0$, whereas in Paper I we neglected the second term (because R_B is large) and thereby reduced it to $B = 0$. We therefore also did a few runs with $B = 0$ here, to verify that the differences really are due to the inclusion of f rather than the different inner boundary condition on B .

As in Paper I, we solve (7–13) using the Hollerbach (2000) code, again with 25×100 modes in r and θ , and again unfortunately with the extremely small time-step of 10^{-7} . However, these values are only for the runs which include poloidal fields. For the purely toroidal runs, one can take timesteps as large as 10^{-5} , and correspondingly also truncations as large as 75×900 . The reason for this is that purely toroidal fields are fundamentally different from mixed poloidal/toroidal fields in the following sense. As noted in Paper I, the numerical difficulties associated with these equations are caused by the feature that the nonlinear Hall term involves two derivatives, just like the linear ohmic term. For purely toroidal fields, however, this is not the case; although the term $\nabla \times [f(\nabla \times \mathbf{B}_t) \times \mathbf{B}_t]$ may look like it involves two derivatives on B , if one works through the algebra, one finds that in fact it does not. It is this difference that makes the purely toroidal equation numerically so much more stable – but, of course, it also calls into question how relevant purely toroidal results are, given how fundamental this difference is. Indeed, we will see below that a surprisingly small ratio of poloidal to toroidal field is already sufficient to yield quite different results.

Finally, we note that the energy equation

$$\frac{\partial}{\partial t} \frac{1}{2} \int \mathbf{B}^2 dV = -R_B^{-1} \int \mathbf{J}^2 dV \quad (14)$$

derived in Paper I still holds, and is again satisfied to within one per cent for all the runs presented here.

3 RESULTS

3.1 Initial condition $\pm B_{l2}$

To facilitate comparison with Vainshtein et al., we start with the purely toroidal results. For our initial condition, we therefore take the $l = 2$ (that is, having angular structure $\sin \theta \cos \theta$) lowest free-decay mode, normalized so that $|B|_{\max} = 1$. This mode is also shown as the initial condition in the top left-hand panels in Figs 2 and 4 below. One reason for considering the equatorially antisymmetric $l = 2$ mode rather than the symmetric $l = 1$ mode is that, as noted in Paper I, the entire subsequent evolution then maintains a definite equatorial symmetry, thereby reducing the computational effort somewhat. As also noted in Paper I, the sign of the toroidal field matters (unlike that of the poloidal field). We will therefore have to consider $\pm B_{l2}$ separately, where the sign of B_{l2} itself is chosen such that B is positive/negative in the northern/southern hemispheres, respectively.

Starting with the initial condition $-B_{l2}$, Fig. 1 shows how the magnetic energy and $|B|_{\max}$ subsequently evolve, for Hall parameters $R_B = 50, 100, 200$ and 400 . We see that the energy decreases monotonically, as of course it must, according to (14). More interestingly, if we consider the dependence on R_B , we note that each subsequent doubling delays the decay by a smaller and smaller amount, with the solutions apparently tending to an R_B -independent limit. That is, the energy decays on the Hall time-scale, rather than on the much longer ohmic time-scale.

In order to understand how this rapid decay comes about, we turn to Fig. 2, showing the detailed structure of the field. The top row shows contours of B at $R_B = 200$, and $t = 0$ (that is, this first panel is the initial condition itself), $0.25, 0.5$ and 0.75 . We see very clearly how the field migrates towards the equator, forming a very thin current sheet there. The second row shows this current sheet in more detail – in particular, its dependence on R_B . In order to deduce precisely how the thickness scales with R_B , the bottom row shows these same plots again, but stretched; whereas the middle row shows wedges extending to 16° from the equator, the bottom row shows $16^\circ, 8^\circ, 4^\circ$ and 2° wedges, stretched to fill the original 16° (that is, the $R_B = 50$ wedge is the same as in the middle row, the $R_B = 100$ wedge has been stretched by a factor of 2, etc.). From the fact that, in these stretched plots, the thickness appears to be tending to an R_B -independent limit, we may deduce that the original, unstretched thickness scales as R_B^{-1} .

Comparing with Vainshtein et al., the agreement is perfect. They showed analytically that for these signs of B , negative in the northern hemisphere and positive in the southern, the field would ‘advect itself’ towards the equator, where the oppositely signed contributions from the two hemispheres would then annihilate themselves in a current sheet of thickness R_B^{-1} [their equation (26), translated into

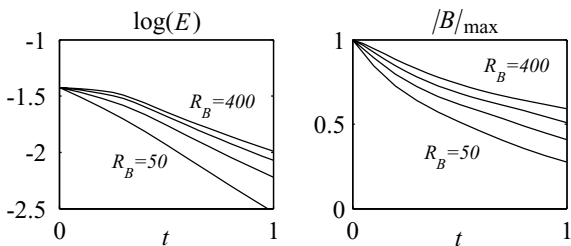


Figure 1. The logarithm of the energy and the maximum value of the field, as functions of time, for the initial condition $-B_{l2}$. $R_B = 50, 100, 200$ and 400 , as indicated.

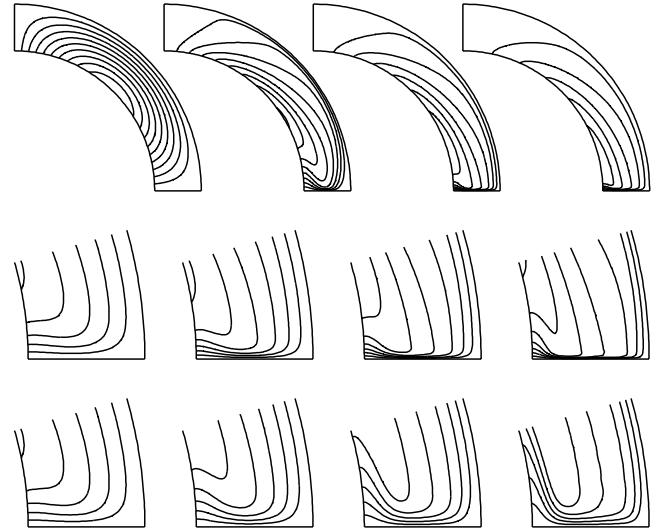


Figure 2. The top row shows the solution at $R_B = 200$, and, from left to right, $t = 0, 0.25, 0.5$ and 0.75 . Note in particular the $\sin \theta \cos \theta$ angular dependence of the initial condition, as well as the $\partial(Br)/\partial r = 0$ (inner) and $B = 0$ (outer) boundary conditions. The boundary conditions (as well as the equatorial antisymmetry) are, of course, preserved throughout the evolution, but the initially simple angular structure is rapidly replaced by this current sheet at the equator. The middle row shows close-ups of the solutions at $t = 0.5$, and, from left to right, $R_B = 50, 100, 200$ and 400 . In the bottom row, these solutions have been blown up even more, by stretching them in θ by factors of 1, 2, 4 and 8, respectively. That is, in the last panel ($R_B = 400$), 2° have been stretched to look like 16° . We see therefore that the current sheet in this case extends to less than 0.5° from the equator. Finally, the contour interval is 0.1 throughout.

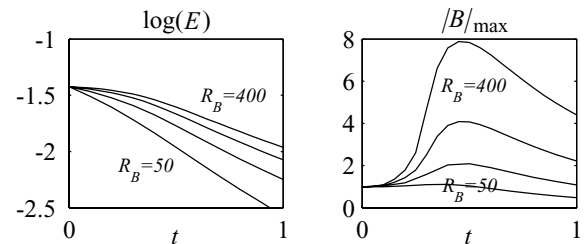


Figure 3. As in Fig. 3, but for the initial condition $+B_{l2}$.

our notation here]. And because this sheet is so thin, the dissipation is fast, on this $O(1)$ Hall time-scale, rather than the $O(R_B)$ ohmic time-scale.

Turning next to the initial condition $+B_{l2}$, Fig. 3 again shows how E and $|B|_{\max}$ subsequently evolve. The decay of the energy again seems to be tending to an R_B -independent limit; indeed, even the details are remarkably similar to the previous results in Fig. 1. In sharp contrast, $|B|_{\max}$ increases very strongly before eventually decaying as well, with the peak amplitude evidently scaling as R_B .

In order to understand this very peculiar behaviour, and, in particular, to see whether ultimately it too can be reconciled with Vainshtein et al. (who found no such increase in $|B|_{\max}$), we again turn to the detailed structure of the field, shown in Fig. 4. As in Fig. 2, the top row shows B at $R_B = 200$, and $t = 0, 0.25, 0.5$ and 0.75 . We see that now the field migrates towards the pole rather than the equator, exactly as predicted by Vainshtein et al. The second row shows this accumulation at the pole in more detail; we note that the

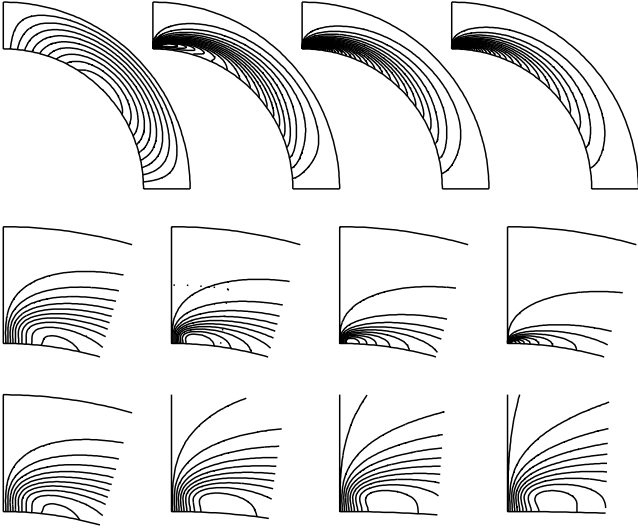


Figure 4. The top row shows the solution at $R_B = 200$, and, from left to right, $t = 0, 0.25, 0.5$ and 0.75 . The middle row shows close-ups of the solutions at $t = 0.5$, and, from left to right, $R_B = 50, 100, 200$ and 400 . In the bottom row, these solutions have been blown up even more, by stretching them in r and θ by factors of 1, 2, 4 and 8, respectively. The dotted lines in the second panel in the middle row show the segment that has been expanded in the bottom row. In the third and fourth panels, even smaller segments have then been expanded, such that the last panel ($R_B = 400$) covers only $1/32$ in r and 2° in θ . This current ‘jet’ therefore extends to roughly 1° from the axis. Finally, the contour interval is 0.1 in the top row, and 0.1, 0.2, 0.4 and 0.8, respectively, in the four panels in the second and third rows, indicating once again how $|B|_{\max}$ scales as R_B .

field develops extremely fine structures in both r and θ this time. The bottom row therefore shows these structures in even more detail, and this time expanded in both r and θ . Once again, the fact that, in these expanded plots, these structures appear to tend to an R_B -independent limit implies that the original thicknesses scale as R_B^{-1} in both r and θ .

So, are these results consistent with Vainshtein et al., who found no increase in $|B|_{\max}$, and predicted that the energy should decay somewhat more slowly than in the case where the field migrates towards the equator? Well, as already noted above, the most basic feature, namely that this time the field moves towards the pole, agrees perfectly. The R_B^{-1} scaling in θ is also exactly as they predicted. Turning next to the R_B^{-1} scaling in r , their model says nothing at all about this, because it is so highly idealized that it is effectively one-dimensional. It is certainly not inconsistent though (nor particularly surprising) to find that a two-dimensional model might also develop fine structures in both dimensions. So, that leaves just this increase in $|B|_{\max}$, and the fact that the energy decays just as quickly as in the previous case. Here, it seems quite clear that both effects can be explained by a geometrical focusing as the field is concentrated at the pole, which first amplifies it, but then also enhances the subsequent decay. Because this geometrical effect was again not included in their model, it is not surprising that they also did not obtain these consequences of it.

We conclude therefore that our results are in perfect agreement with Vainshtein et al. for both initial conditions $-\mathbf{B}_{l2}$ and $+\mathbf{B}_{l2}$: for the former, the field ‘advects itself’ towards the equator; for the latter, towards the pole. In both cases, extremely fine structures, scaling as R_B^{-1} , develop in θ (and in r as well for $+\mathbf{B}_{l2}$), as a result of which the field decays on the Hall time-scale rather than the much longer ohmic time-scale.

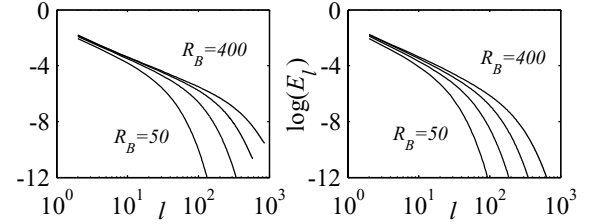


Figure 5. Power spectra as functions of the spherical harmonic degree l , at $t = 0.5$, for $-\mathbf{B}_{l2}$ on the left and $+\mathbf{B}_{l2}$ on the right.

Finally, Fig. 5 shows the power spectra in the two cases. We note the dissipative cut-off at $l = O(R_B)$ in both cases, exactly as expected. We also note that $-\mathbf{B}_{l2}$ has even more structure at high l than $+\mathbf{B}_{l2}$ does; this too is exactly as expected, given that for $R_B = 400$, for example, the finest structures in the two cases span 0.5° and 1° , respectively (as noted in Figs 2 and 4).

3.2 Initial condition \mathbf{B}_{p1}

To see now how things change when we include a poloidal field, we take the initial condition \mathbf{B}_{p1} , the $l = 1$ (having angular structure $\sin \theta$) lowest free-decay mode previously introduced in Paper I (and as in Paper I, the sign of the poloidal field makes no difference). According to (8), this will immediately induce a toroidal field as well, which, according to the symmetry properties noted in I, will have the same equatorial symmetry as \mathbf{B}_{l2} . The left-hand panel in Fig. 6 shows the maximum amplitude of this induced toroidal field, which we note consists of a very rapid increase followed by a more gradual decay. Now, it turns out that the sign of this toroidal field is negative/positive in the northern/southern hemisphere, that is, just like $-\mathbf{B}_{l2}$. Based on our previous results, therefore, we would expect this toroidal field to advect everything towards the equator, where it should again annihilate itself in this very thin current sheet.

However, if we now turn to the right-hand panel in Fig. 6, we find that the energy does not decay on the Hall time-scale. There is an initial adjustment that does take place on the Hall time-scale (corresponding to this establishment of B shown in the left-hand panel), but thereafter the energy decreases on the ohmic time-scale. We note though that it is nevertheless considerably faster than the ohmic decay rate of \mathbf{B}_{p1} by itself.

In order to understand why this Vainshtein et al. mechanism does not appear to be operating in this case, or, at least, not nearly as efficiently as before, we again need to consider the detailed structure of the field, shown in Fig. 7. The first row shows the poloidal field

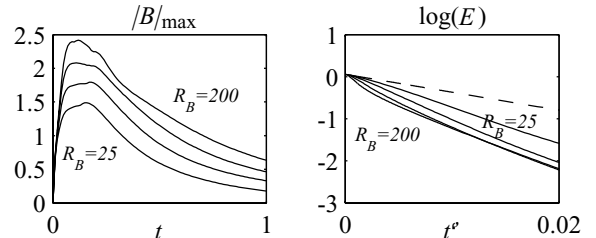


Figure 6. On the left, $|B|_{\max}$ as a function of time, for the initial condition \mathbf{B}_{p1} . This panel is therefore just as in Figs 1 and 3. The panel on the right is different though, showing the energy as a function of $t' = t/R_B$ – that is, on the ohmic time-scale rather than the Hall time-scale. The dashed line shows how \mathbf{B}_{p1} would decay if ohmic decay alone were acting.

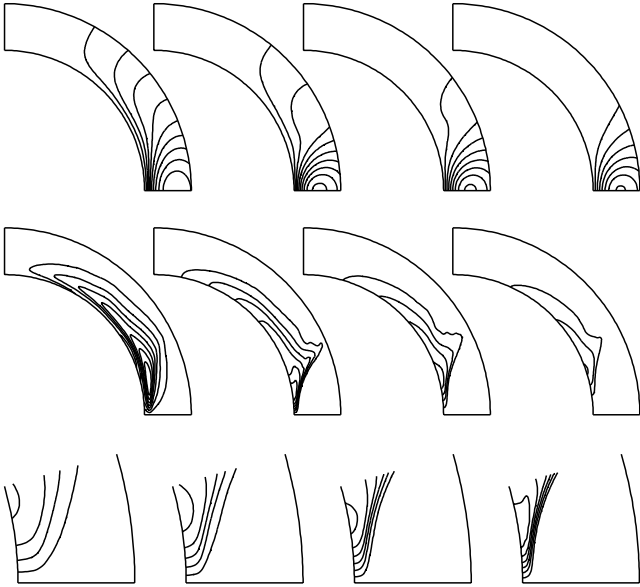


Figure 7. The first and second rows show the poloidal and toroidal fields, respectively, for $R_B = 200$, and, from left to right, $t = 0.1, 0.25, 0.5$ and 0.75 . Once again, the initial condition was a purely poloidal field having a $\sin\theta$ angular dependence. We see therefore how a toroidal field is *very* rapidly induced, and immediately starts ‘compressing’ the poloidal field into the equatorial region. The bottom row shows close-ups of the toroidal field at $t = 0.25$, and, from left to right, $R_B = 25, 50, 100$ and 200 . The contour interval is 0.05 for the poloidal fields and 0.3 for the toroidal. Recall also that A is equatorially symmetric and B is antisymmetric. Finally, we note that the only part of all of this evolution that would be visible from the outside is the external potential field to which A matches.

and the second row shows the toroidal field, for $R_B = 200$, and $t = 0.1, 0.25, 0.5$ and 0.75 . At $t = 0.1$, the poloidal field is therefore still very much like its initial condition \mathbf{B}_{p1} , but it has now induced this toroidal field as well, which, as already noted above, is negative in this hemisphere. We expect therefore that it will at least attempt to advect everything towards the equator, as indeed it does. However, it does not succeed in reaching the equator; once the poloidal field has been ‘compressed’ by a certain amount, it resists further advection of either field component. The toroidal field therefore does not set up a current sheet at the equator, but does so somewhat earlier instead.

Now, one might think that it doesn’t much matter where B sets up this current sheet; it will still lead to a rapid dissipation of the energy. However, if one looks at this sheet in more detail, one finds that its dependence on R_B is weaker than before, as shown in the bottom row in Fig. 7. More quantitatively, if one computes the maximum values of $|\nabla B|$, one obtains 15, 36, 69 and 113, for $R_B = 25, 50, 100$ and 200 , respectively. The successive ratios $36/15 = 2.4$, $69/36 = 1.9$ and $113/69 = 1.6$ are unfortunately less than conclusive, but are perhaps tending towards $\sqrt{2}$, which would imply an $R_B^{-1/2}$ scaling for the thickness of the current sheet in this case. However, if the current sheet is not as thin as it was before, it is also not as efficient at dissipating the field, explaining why the decay in this case is still on the ohmic time-scale rather than on the Hall time-scale. Of course, the fact that it does decay significantly faster than just the free decay rate of \mathbf{B}_{p1} by itself is also easy to understand; these very short length-scales that have been generated do enhance the decay rate after all, even if it is ultimately still on the ohmic time-scale.

Finally, Fig. 8 again shows power spectra of these solutions. The poloidal field shows a certain break around $l = 15$ or so, correspond-

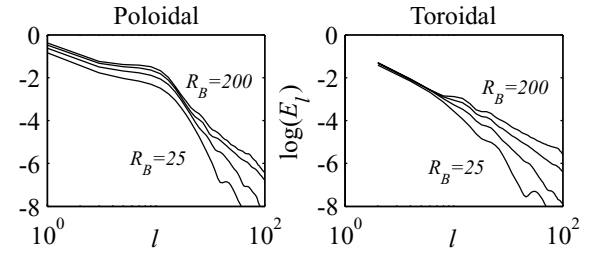


Figure 8. Power spectra as functions of the spherical harmonic degree l , at $t = 0.25$.

ing to the degree to which it has been compressed into the equatorial region. However, the more important point to note is that, very much unlike Fig. 5, there is now no evidence of a definite dissipative cut-off. As noted in Paper I, in this more general case, where the Hall term has two derivatives just like the ohmic term, one obtains a definite dissipative cut-off only if the coupling is purely local in wavenumber space. The absence of a dissipative cut-off therefore indicates that the coupling is not localized in this way (as was also the case in Paper I).

3.3 Initial condition $\pm\mathbf{B}_{l2} + \epsilon\mathbf{B}_{p1}$

The results presented in the previous two sections are unfortunately rather different; whereas purely toroidal fields decay on the Hall time-scale, poloidal initial conditions only decay on the much longer ohmic time-scale. In order to assess which set of results is likely to be more relevant to real neutron stars, we therefore consider initial conditions of the form $\pm\mathbf{B}_{l2} + \epsilon\mathbf{B}_{p1}$, and simply see how large ϵ can be before the field no longer decays on the Hall time-scale.

Fig. 9 shows the results for $-\mathbf{B}_{l2} + 0.3\mathbf{B}_{p1}$. We see that initially the poloidal field again manages to prevent the toroidal field from reaching the equator. Eventually, however, the toroidal field overwhelms the poloidal – we note, for example, how the poloidal field has been almost completely annihilated by $t = 1$ – and thereafter does manage to establish a current sheet on the equator. Not surprisingly, the subsequent evolution is then much like the purely toroidal case, with the energy decaying on the Hall time-scale. It is crucial though that ϵ should be at most 0.3 ; for larger values, the toroidal

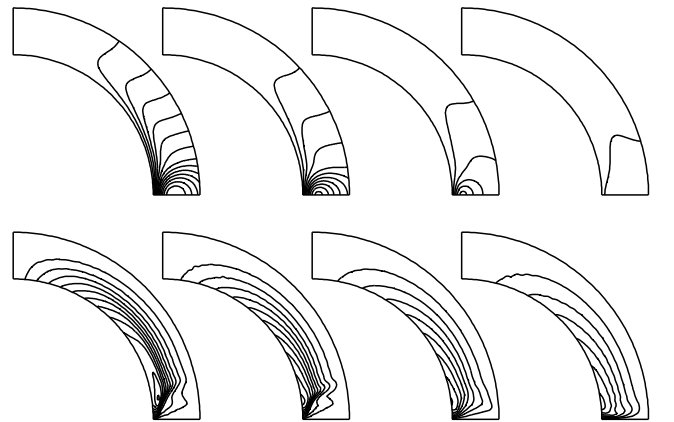


Figure 9. Contour plots of the poloidal (upper) and toroidal (lower) fields for the initial condition $-\mathbf{B}_{l2} + 0.3\mathbf{B}_{p1}$. $R_B = 200$, and, from left to right, $t = 0.25, 0.5, 0.75$ and 1 . The contour intervals are 0.01 (upper) and 0.1 (lower).

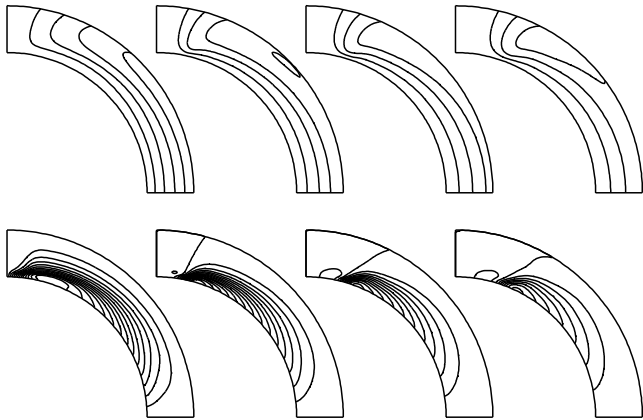


Figure 10. As in Fig. 9, but for the initial condition $\mathbf{B}_{l2} + 0.05\mathbf{B}_{p1}$. The contour intervals are 0.005 (upper) and 0.1 (lower). The toroidal field is negative near the pole and positive everywhere else. Note also how all of the external poloidal field emerges in the polar region; this is a point we will return to in the conclusion.

field never manages to overwhelm the poloidal, and the evolution is as in Fig. 7 rather than Fig. 2.

Next, Fig. 10 shows the results for $\mathbf{B}_{l2} + 0.05\mathbf{B}_{p1}$. Because ϵ is now so small, the negative toroidal field induced by \mathbf{B}_{p1} is overwhelmed by the positive contribution from \mathbf{B}_{l2} itself. Therefore, we would expect the evolution to be towards the pole, as in Fig. 4. Indeed, that is exactly what happens. However, very much unlike Fig. 4, it never reaches the pole. As the poloidal field gets compressed into the polar regions, its effect becomes enhanced, to the point where it is able to induce a small region of negative B , which then blocks any further migration towards the pole. And as before, the scalings of these fine structures are sufficiently altered that they are no longer as effective in dissipating the field, with the result that the decay is again on the ohmic time-scale rather than the Hall time-scale.

4 CONCLUSION

The results presented here demonstrate that the combination of Hall drift and stratification significantly influences the evolution of a neutron star's magnetic field, and indeed in ways that are quite different from what Hall drift without stratification (Paper I) would have yielded. The precise details, however, depend crucially on the details of the initial field. The two key features seem to be (i) the sign of the toroidal field in the two hemispheres and (ii) the ratio of poloidal to toroidal field.

Regarding the sign of B , we obtained results in perfect agreement with the analytic model of Vainshtein et al., namely that depending on the signs in the two hemispheres, the field will migrate towards either the equator or the pole. Just as in their model, a purely toroidal field will then dissipate on the fast Hall time-scale in either case. When we included poloidal fields though, we found that a surprisingly small amount could already be sufficient to disrupt this fast dissipation.

However, in retrospect, this should probably not be so surprising after all, for the following reason. As noted above, for purely toroidal fields, the Hall term only has one derivative, whereas for the full problem, it has two. If this second derivative comes entirely from the poloidal field though, then any amount of poloidal field will become important, if one just considers sufficiently short length-scales. That is, it is precisely in the detailed structure of these current sheets (which one needs if one is to have any hope of achieving fast

dissipation) that one would expect even a very weak poloidal field to have a significant influence. Indeed, if we could achieve larger values of R_B , it seems likely that even weaker poloidal fields would already be important, because then the relevant length-scales also become shorter.

Finally, what might all this imply for real neutron stars? We begin by noting that the correct poloidal/toroidal ratio is unfortunately not known, because the details of when, where and how the 'initial condition' is generated in the first place are not known for certain. Thompson & Duncan (1993) consider the possibility of dynamo action, either in the final stages of the progenitor star, or in the very early stages of the neutron star. Alternatively, Blandford, Applegate & Hernquist (1983) – see also Wiebicke & Geppert (1996) – suggest that it may result from the so-called thermo-electric effect, again acting early in the neutron star's life. All of these effects are likely to generate considerable toroidal fields, but the precise strength could vary considerably. For example, Thompson & Duncan note that differential rotation, which of course generates toroidal field from poloidal, is likely to be less important if the dynamo acts in the neutron star itself rather than the precursor.

It seems plausible therefore that the toroidal field might be stronger than the poloidal field, but precisely how much is unknown. According to the results presented here, it is thus possible that two superficially similar neutron stars could nevertheless evolve very differently, with one exhibiting rapid field decay but the other not, just as Figs 7 and 9 start out very similar, before the poloidal field suddenly collapses in Fig. 9 but not in 7. Indeed, on the basis of the results presented here, one might be able to use the observed decay rate to infer something about the poloidal/toroidal field ratio.

As interesting as this contrast between Figs 7 and 9 is, that between Figs 9 and 10 is perhaps even more remarkable. In particular, this most basic feature, that the sign of the toroidal field in the two hemispheres dictates whether the migration (of both field components) is towards the poles or the equator, could be quite important, for the following reason. The strength of a pulsar's signal is determined at least in part by how narrowly focused its beam is, which, in turn, is determined by the structure of the magnetic field. So if the field is concentrated at the poles, rather than dispersed around the equator, the signal is also likely to be stronger. How visible a pulsar is may therefore be affected by something as seemingly unrelated as the orientation of its internal toroidal field.

ACKNOWLEDGMENT

RH's stay in Germany was made possible by a Research Fellowship of the Alexander von Humboldt Foundation.

REFERENCES

- Blandford R. D., Applegate J. H., Hernquist L., 1983, MNRAS, 204, 1025
- Goldreich P., Reisenegger A., 1992, ApJ, 395, 250
- Hollerbach R., 2000, Int. J. Numer. Meth. Fluids, 32, 773
- Hollerbach R., Rüdiger G., 2002, MNRAS, 337, 216
- Jones P. B., 1988, MNRAS, 233, 875
- Shalybkov D. A., Urpin V. A., 1997, A&A, 321, 685
- Shapiro S., Teukolsky S., 1983, Black Holes, White Dwarfs and Neutron Stars. Wiley, New York
- Thompson C., Duncan R. C., 1993, ApJ, 408, 194
- Urpin V., Shalybkov D., 1999, MNRAS, 304, 451
- Vainshtein S. I., Chitre S. M., Olinato A. V., 2000, Phys. Rev. E, 61, 4422
- Wiebicke H. J., Geppert U., 1996, A&A, 309, 203

This paper has been typeset from a $\text{\TeX}/\text{\LaTeX}$ file prepared by the author.